

UC Berkeley

UC Berkeley Previously Published Works

Title

LY α FOREST TOMOGRAPHY FROM BACKGROUND GALAXIES: THE FIRST MEGAPARSEC-RESOLUTION LARGE-SCALE STRUCTURE MAP AT $z > 2$

Permalink

<https://escholarship.org/uc/item/9md0h0x6>

Journal

The Astrophysical Journal Letters, 795(1)

ISSN

2041-8205

Authors

Lee, Khee-Gan
Hennawi, Joseph F
Stark, Casey
[et al.](#)

Publication Date

2014-11-01

DOI

10.1088/2041-8205/795/1/l12

Peer reviewed

LY α FOREST TOMOGRAPHY FROM BACKGROUND GALAXIES:
THE FIRST MEGAPARSEC-RESOLUTION LARGE-SCALE STRUCTURE MAP AT $z > 2$

KHEE-GAN LEE¹, JOSEPH F. HENNAWI¹, CASEY STARK^{2,3}, J. XAVIER PROCHASKA^{4,5}, MARTIN WHITE^{2,3},
DAVID J. SCHLEGEL⁵, ANNA-CHRISTINA EILERS¹, ANDREU ARINYO-I-PRATS⁶, NAO SUZUKI⁷, RUPERT A.C. CROFT⁸,
KARINA I. CAPUTI⁹, PAOLO CASSATA^{10,11}, OLIVIER ILBERT¹¹, BIANCA GARILLI¹², ANTON M. KOEKEMOER¹³,
VINCENT LE BRUN¹¹, OLIVIER LE FÈVRE¹¹, DARIO MACCAGNI¹⁵, PETER NUGENT^{3,2}, YOSHIAKI TANIGUCHI¹⁴,
LIDIA A.M. TASCA¹¹, LAURENCE TRESSE¹¹, GIANNI ZAMORANI¹⁵, ELENA ZUCCA¹⁵

Accepted for ApJL

ABSTRACT

We present the first observations of foreground Lyman- α forest absorption from high-redshift galaxies, targeting 24 star-forming galaxies (SFGs) with $z \sim 2.3$ – 2.8 within a $5' \times 15'$ region of the COSMOS field. The transverse sightline separation is $\sim 2 h^{-1}$ Mpc comoving, allowing us to create a tomographic reconstruction of the 3D Ly α forest absorption field over the redshift range $2.20 \leq z \leq 2.45$. The resulting map covers $6 h^{-1}$ Mpc \times $14 h^{-1}$ Mpc in the transverse plane and $230 h^{-1}$ Mpc along the line-of-sight with a spatial resolution of $\approx 3.5 h^{-1}$ Mpc, and is the first high-fidelity map of large-scale structure on \sim Mpc scales at $z > 2$. Our map reveals significant structures with $\gtrsim 10 h^{-1}$ Mpc extent, including several spanning the entire transverse breadth, providing qualitative evidence for the filamentary structures predicted to exist in the high-redshift cosmic web. Simulated reconstructions with the same sightline sampling, spectral resolution, and signal-to-noise ratio recover the salient structures present in the underlying 3D absorption fields. Using data from other surveys, we identified 18 galaxies with known redshifts coeval with our map volume enabling a direct comparison to our tomographic map. This shows that galaxies preferentially occupy high-density regions, in qualitative agreement with the same comparison applied to simulations. Our results establishes the feasibility of the CLAMATO survey, which aims to obtain Ly α forest spectra for ~ 1000 SFGs over $\sim 1 \text{ deg}^2$ of the COSMOS field, in order to map out IGM large-scale structure at $\langle z \rangle \sim 2.3$ over a large volume $(100 h^{-1} \text{ Mpc})^3$.

Subject headings: cosmology: observations — galaxies: high-redshift — intergalactic medium — quasars: absorption lines — surveys — techniques: spectroscopic

1. INTRODUCTION

lee@mpia.de

¹ Max Planck Institute for Astronomy, Königstuhl 17, D-69117 Heidelberg, West Germany

² Department of Astronomy, University of California at Berkeley, B-20 Hearst Field Annex # 3411, Berkeley, CA 94720, USA

³ Lawrence Berkeley National Laboratory, 1 Cyclotron Rd., Berkeley, CA 94720, USA

⁴ Department of Astronomy and Astrophysics, University of California, 1156 High Street, Santa Cruz, CA 95064, USA

⁵ University of California Observatories, Lick Observatory 1156 High Street, Santa Cruz, CA 95064, USA

⁶ Institut de Ciències del Cosmos, Universitat de Barcelona (IEEC-UB), Martí Franquès 1, E08028 Barcelona, Spain

⁷ Kavli Institute for the Physics and Mathematics of the Universe (IPMU), The University of Tokyo, Kashiwanoha 5-1-5, Kashiwa-shi, Chiba, Japan

⁸ Department of Physics, Carnegie-Mellon University, 5000 Forbes Avenue, Pittsburgh, PA 15213, USA

⁹ Kapteyn Astronomical Institute, University of Groningen, P.O. Box 800, 9700 AV Groningen, The Netherlands

¹⁰ Instituto de Física y Astronomía, Facultad de Ciencias, Universidad de Valparaíso, Av. Gran Bretaña 1111, Casilla 5030, Valparaíso, Chile

¹¹ Aix Marseille Université, CNRS, LAM (Laboratoire d'Astrophysique de Marseille) UMR 7326, 13388, Marseille, France

¹² INAF-IASF, via Bassini 15, I-20133, Milano, Italy

¹³ Space Telescope Science Institute, 3700 San Martin Drive, Baltimore MD 21218, USA

¹⁴ Research Center for Space and Cosmic Evolution, Ehime University, 2-5 Bunkyo-cho, Matsuyama 790-8577, Japan

¹⁵ INAF-Osservatorio Astronomico di Bologna, via Ranzani, 1, I-40127, Bologna, Italy

The Lyman- α (Ly α) ‘forest’ absorption seen in quasar spectra is a crucial probe of the intergalactic medium (IGM). In the modern ‘fluctuating Gunn-Peterson’ scenario (Cen et al. 1994; Bi et al. 1995; Croft et al. 1998; Hui et al. 1997), this is from residual neutral hydrogen in photoionization-equilibrium, tracing the underlying density field, allowing the study of large-scale structure (LSS) at $z \gtrsim 2$ (e.g., Croft et al. 2002; McDonald et al. 2006; Busca et al. 2013; Palanque-Delabrouille et al. 2013; Delubac et al. 2014).

The Ly α forest observed in individual quasars probe the IGM along 1-dimension, but using multiple spectra with small transverse separations, it is possible to ‘tomographically’ reconstruct a 3D map of the Ly α forest absorption (Pichon et al. 2001; Caucci et al. 2008; Cisewski et al. 2014; Lee et al. 2014a, hereafter L14). The effective spatial-resolution, ϵ_{3D} , of such a map is determined by the transverse sightline separation, $\langle d_{\perp} \rangle$. This probes \sim Mpc scales only by exploiting UV-bright star-forming galaxies (SFGs) as background sources in addition to quasars. However, SFGs are faint ($g \gtrsim 23$) — even with 8-10m telescopes, only spectral S/N of a few are feasible from such objects, assuming reasonable exposure times. However, L14 argued that such data at moderate resolutions ($R \equiv \lambda/\Delta(\lambda) \sim 1000$) are adequate for Ly α forest tomography that resolve the LSS on scales of $\epsilon_{3D} \sim 2 - 5 h^{-1}$ Mpc.

In this Letter, we describe pilot observations for the

COSMOS Lyman-Alpha Mapping And Tomography Observations (CLAMATO) survey. The full survey is aimed at mapping the $z \sim 2.3$ IGM within $\sim 1 \text{ deg}^2$ of the COSMOS field (Scoville et al. 2007). The pilot observations were however limited to one half-night of successful data, yielding moderate-resolution spectra for 24 SFGs at $g \leq 24.9$ within $\sim 5' \times 14'$.

This data represents, to our knowledge, the first systematic attempt to exploit spectra of unlensed high-redshift SFGs for Ly α forest analysis. Our background sources are $\sim 2.5 - 3 \text{ mag}$ fainter than existing Ly α forest datasets (e.g., $g \sim 21.5$ in BOSS, Dawson et al. 2013), yielding ~ 100 greater area density of sightlines ($\sim 1000 \text{ deg}^{-2}$ vs $\sim 15 \text{ deg}^{-2}$ in BOSS). This dramatic increase results in small average inter-sightline separations ($\langle d_{\perp} \rangle \sim 2.3 h^{-1} \text{ Mpc}$), enabling a tomographic reconstruction of the 3D Ly α forest absorption, providing an unprecedented view of the $z > 2$ cosmic web on scales of several comoving Mpc. As we shall see, comparisons with a small number of coeval galaxies as well as simulated reconstructions indicate that the map is indeed tracing LSS.

In this paper, we assume a concordance flat Λ CDM cosmology with $\Omega_M = 0.26$, $\Omega_{\Lambda} = 0.74$, and $H_0 = 70 \text{ km s}^{-1}$.

2. OBSERVATIONS AND DATA REDUCTION

Our observations target g -selected galaxies and AGN (using the Capak et al. 2007 photometry) at $2.3 < z_{\text{bg}} < 3$, such that their Ly α forest absorption covers $2.15 \leq z_{\alpha} \leq 2.40$. By working in the COSMOS field (Scoville et al. 2007), we are able to exploit rich multiwavelength imaging and spectroscopy to efficiently target the necessary background sources. Our primary candidates are spectroscopically-confirmed objects from the zCOSMOS-Deep (Lilly et al. 2007) and VUDS (Le Fevre et al. 2014) surveys — we reobserve these to obtain adequate S/N and spectral resolution for tomography. Where available, we also added grism redshifts kindly provided by the 3D-HST team (e.g. Brammer et al. 2012). Beyond spectroscopically-confirmed candidates, we add photometric redshifts from Ilbert et al. (2009) as well as Salvato et al. (2011) for X-ray detected sources. From these candidates, we selected targets based on redshift probability, source brightness, and uniformity on the sky — the selection functions of the source catalogs are unimportant to us since the background source properties do not bias the foreground absorption.

We observed with the LRIS Double-Spectrograph (Oke et al. 1995; Steidel et al. 2004) on the Keck-I telescope at Mauna Kea, Hawai'i, during 2014 March 26-27 and 29-30, in MOS mode with the B600/4000 grism on the blue arm and R600/5000 grating on the red with the d500 dichroic. With $1''$ slits, this yields $R \equiv \lambda/\Delta\lambda \approx 1000$ and $R \approx 1200$ for the blue and red arms, respectively. We suffered a $\sim 70\%$ weather loss, but obtained good-quality spectra for 2 slitmasks covering $\sim 5' \times 15'$, with total exposure times of 6600-7200s in $0.5 - 0.7''$ seeing and clear conditions. These two slitmasks overlap along their short edge, resulting in an elongated footprint (Figure 1).

The data was reduced with the XIDL package¹⁶, and visually-inspected to determine source redshifts. Out of 47 targeted objects, we successfully extracted 1D spectra and estimated redshifts for 33, of which 24 were determined to have the correct redshift and adequate spectral S/N to contribute to our tomographic reconstruction. The number of sources within our nominal $g \leq 24.5$ survey limit is $\sim 50\%$ that estimated by L14, a shortfall that was already evident during the target-selection process. This is likely because L14 did not take into account dust-reddening ($E(B - V) \sim 0.2$, Reddy et al. 2008) when estimating source counts — the SFG luminosity function is so steep that even small errors in the assumed magnitudes could easily lead to this $\sim 50\%$ discrepancy. To fill the slitmasks, we therefore also targeted $g > 24.5$ objects but these were less likely to be successfully reduced or have adequate S/N. Nevertheless, even this reduced number of sources is sufficient to carry out Ly α forest tomography, as we shall see.

The position of the 24 SFGs on the sky are shown in Figure 1. Our brightest objects are $g \approx 24.0$ SFGs with $S/N \approx 3 - 4$ per 1.2 \AA pixel, while on the faint-end we use spectra down to $S/N \approx 1.3$ from $g \approx 24.8$ sources. Examples of the spectra are shown in Figure 2. We also attempted to visually identify damped Ly α absorbers that might affect Ly α forest analysis but found none.

To extract the Ly α forest transmission from the spectra, we need to estimate the intrinsic ‘continuum’ of the SFGs. Studies of $z \sim 3$ SFG composite spectra (Shapley et al. 2003; Berry et al. 2012) suggest that this is relatively flat in the Ly α forest region, with only a few strong intrinsic absorbers visible — this is corroborated by high-resolution line analysis of the lensed galaxy MS1512-cB58 (Savaglio et al. 2002). From these studies, we determined that the strongest intrinsic absorption within the $1040 - 1190 \text{ \AA}$ Ly α forest region are at N II $\lambda 1084.0$, N I $\lambda 1134.4$, and C III $\lambda 1175.7$ — we mask $\pm 5 \text{ \AA}$ around these transitions. We then adopt as our continuum template the restframe composite spectrum of 59 SFGs from Berry et al. (2012), in which the Ly α forest variance in the restframe $\sim 1040 - 1190 \text{ \AA}$ region have been smoothed out through averaging, albeit with an overall absorption decrement.

Using this template, we estimate the continuum, C , for each individual spectrum by ‘mean-flux regulation’ (Lee et al. 2012, 2013), i.e. adjusting the amplitude and slope of the $1040 - 1190 \text{ \AA}$ continuum template until the mean Ly α forest transmission, $\langle F \rangle(z)$, from each spectrum agrees with the measurements of Becker et al. (2013). This method ensures that there is no overall bias in the resulting continua. We estimate the continuum error to be $\lesssim 10\%$, by considering the variation of Starburst99 (Leitherer et al. 1999, 2010) models with respect to various physical parameters. This is adequate for our $S/N \leq 4$ spectra, but in future papers we will study SFG continuum-fitting in more detail.

We divide the restframe $1040 - 1190 \text{ \AA}$ flux, f , from each spectrum by the continuum to obtain the Ly α forest transmission $F = f/C$, and further the forest fluctuations:

$$\delta_F = F/\langle F \rangle(z) - 1. \quad (1)$$

¹⁶ http://www.ucolick.org/~xavier/LowRedux/lris_cook.html

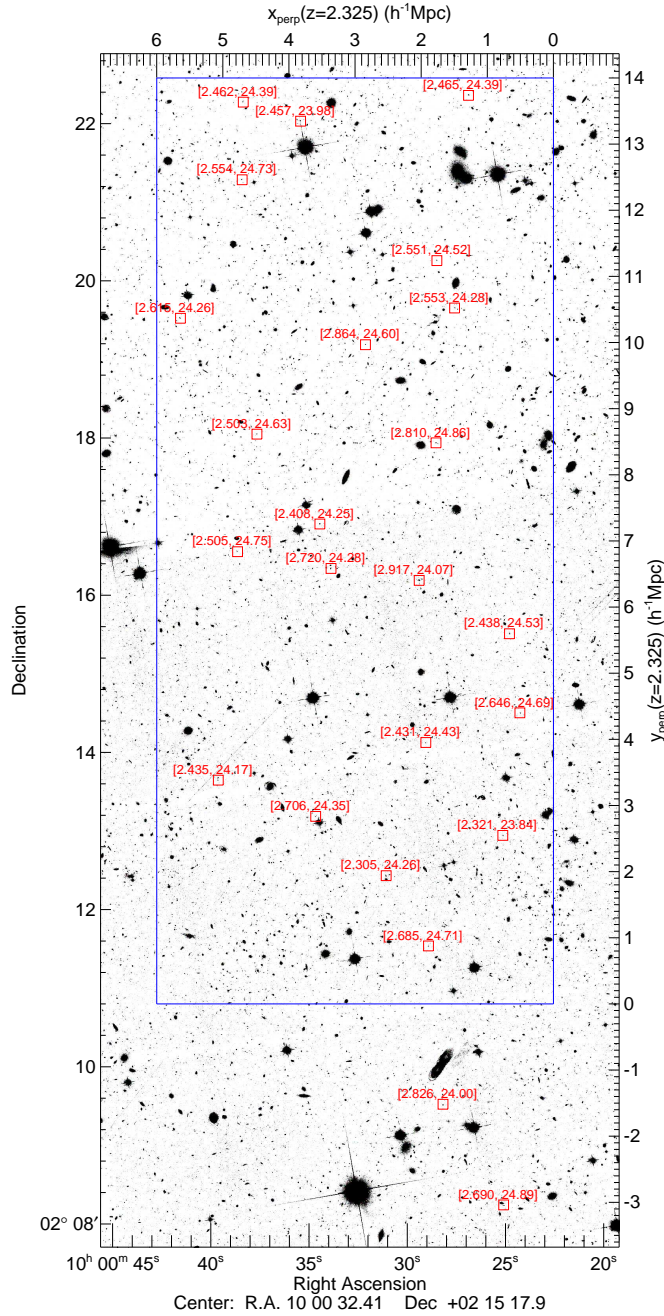


FIG. 1.— HST ACS F814W mosaic (Koekemoer et al. 2007) of our target region. The red boxes indicate our background spectroscopic sources with Ly α forest coverage over $2.15 \leq z_{\alpha} \leq 2.40$; source redshifts and g -magnitudes are labeled above each object. The transverse area of our map is bounded in blue; upper- and right-axes indicate the transverse comoving separation at $z = 2.325$ relative to the map coordinate origins.

We also compute the error, $\sigma_N = \sigma/C/\langle F \rangle(z)$, where σ is the pixel noise reported by the reduction pipeline. The vectors of δ_F and σ_N , along with the corresponding 3D pixel positions, constitute the inputs for the tomographic reconstruction.

3. TOMOGRAPHIC RECONSTRUCTION

To create the Ly α forest tomographic reconstruction, we use Wiener filtering (e.g., Wiener 1942; Press et al. 1992; Zaroubi et al. 1995), where the reconstructed field, δ_F^{rec} , is:

$$\delta_F^{\text{rec}} = \mathbf{C}_{\text{MD}} \cdot (\mathbf{C}_{\text{DD}} + \mathbf{N})^{-1} \cdot \delta_F, \quad (2)$$

where $\mathbf{C}_{\text{DD}} + \mathbf{N}$ and \mathbf{C}_{MD} are the data-data and map-data covariances, respectively. The noise covariance matrix \mathbf{N} is assumed to have only diagonal elements set by the noise variances, $N_{ii} = \sigma_{N,i}^2$. This term allows us to weight each input pixel by its S/N, so lower-S/N spectra are down-weighted and avoids noise spikes from biasing the map.

Following L14 and Caucci et al. (2008), we assume that between any two points \mathbf{r}_1 and \mathbf{r}_2 , whether in the maps

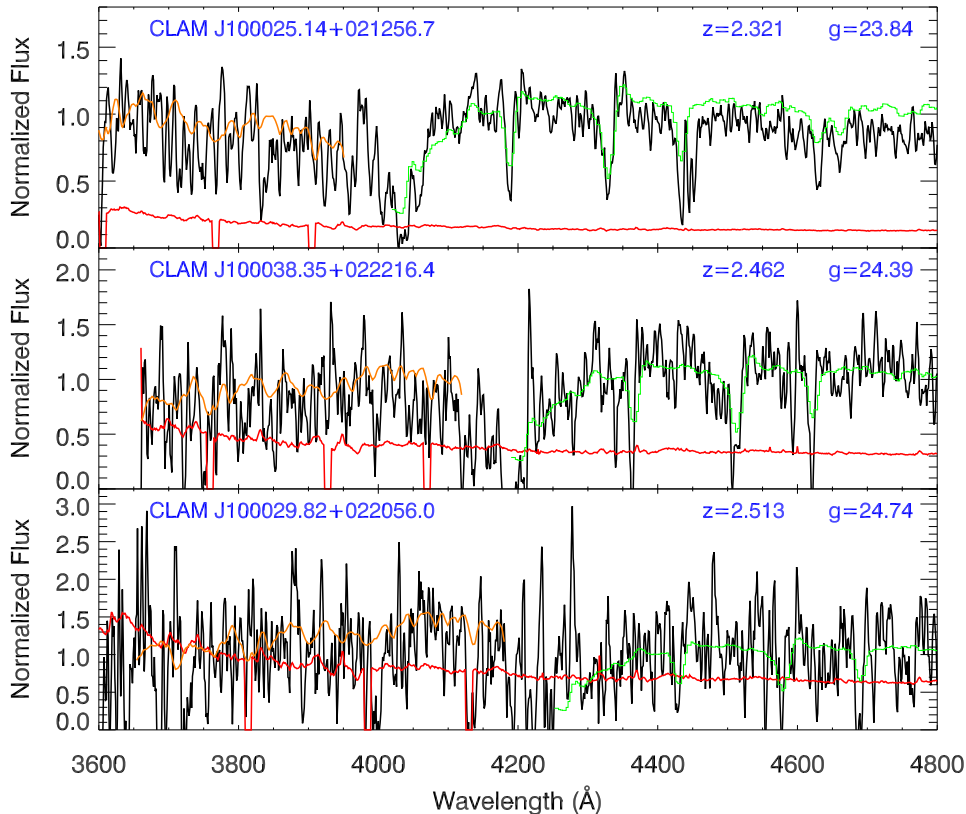


FIG. 2.— Examples of SFG spectra obtained with Keck-LRIS and subsequently used for Ly α forest tomographic reconstruction. From top to bottom, these represent our highest-, median-, and lowest-S/N spectra, respectively. The red curve represents the estimated pixel noise, with masked pixels (mostly intrinsic absorption-lines) set to zero. The green curve is the Shapley et al. (2003) composite LBG spectrum overplotted at the source redshifts, while the orange curve is the estimated continuum (see text).

or skewers, $\mathbf{C}_{\text{DD}} = \mathbf{C}_{\text{MD}} = \mathbf{C}(\mathbf{r}_1, \mathbf{r}_2)$ and

$$\mathbf{C}(\mathbf{r}_1, \mathbf{r}_2) = \sigma_F^2 \exp \left[-\frac{(\Delta r_{\parallel})^2}{2L_{\parallel}^2} \right] \exp \left[-\frac{(\Delta r_{\perp})^2}{2L_{\perp}^2} \right], \quad (3)$$

where Δr_{\parallel} and Δr_{\perp} are the distance between \mathbf{r}_1 and \mathbf{r}_2 along, and transverse to, the line-of-sight, respectively. L_{\parallel} and L_{\perp} are free parameters that set the effective smoothing of the reconstruction parallel and perpendicular to the line-of-sight, respectively, while $\sigma_F = 0.8$ sets the overall correlation strength. These parameters need to be matched to the data quality: we set $L_{\parallel} = 2.7 h^{-1}$ Mpc, roughly the comoving scale along the LOS corresponding to our spectral resolution element. For L_{\perp} , Caucci et al. (2008) suggested setting it to the typical transverse sightline separation $\langle d_{\perp} \rangle$, but we choose $L_{\perp} = 3.5 h^{-1}$ Mpc even though our sightline separation is $\langle d_{\perp} \rangle \approx 2.3 h^{-1}$ Mpc. This is a conservative choice taking into account the low-S/N of our individual spectra. The choice of these reconstruction parameters is somewhat arbitrary since small changes do not qualitatively change the resulting map features, but in future work we will discuss optimal choices for these parameters.

Our map originates at $[\alpha_0, \delta_0] = [10^h 00' 22^s.56, +02^{\circ} 10' 48.0'']$, spanning

$[6h^{-1} \text{ Mpc}, 14h^{-1} \text{ Mpc}]$ in the $[x_{\text{perp}}, y_{\text{perp}}]$ directions on the sky (c.f. top- and right-axes in Figure 1); along the line-of-sight, the origin is $z_{\alpha} = 2.20$ and extends $\Delta\chi = 230 h^{-1}$ Mpc up to $z_{\alpha} \approx 2.45$, giving an overall comoving volume of $6 h^{-1} \text{ Mpc} \times 14 h^{-1} \text{ Mpc} \times 230 h^{-1} \text{ Mpc} = 19320 h^{-3} \text{ Mpc}^3 \approx (27 h^{-1} \text{ Mpc})^3$. Note that our map does not cover the region $\delta \lesssim 2^{\circ} 11'$, where we experienced a high failure-rate in spectral-extraction and redshift-identification due to deteriorating observing conditions. However, the two spectra in the excluded region are still included in the map input; given our transverse correlation length of $L_{\perp} = 3.5 h^{-1}$ Mpc, these spectra ($\approx 1.5 h^{-1}$ Mpc and $\approx 3 h^{-1}$ Mpc from the lower map boundary) still contribute to the low- y_{perp} portions of the map.

We evaluated Equation 2 to solve for the output tomographic map, δ_F^{rec} , using a preconditioned conjugate-gradient algorithm to carry out the matrix inversion and matrix-vector multiplication (C. Stark et al., in preparation), sampling on a 3D comoving grid with $(0.5 h^{-1} \text{ Mpc})^3$ cells. For simplicity, we assumed a fixed differential comoving distance $d\chi/dz$ (evaluated at $z = 2.325$, the mean map redshift) when setting up the output grid. This avoids a flared map geometry, since the transverse comoving area increases with redshift, but

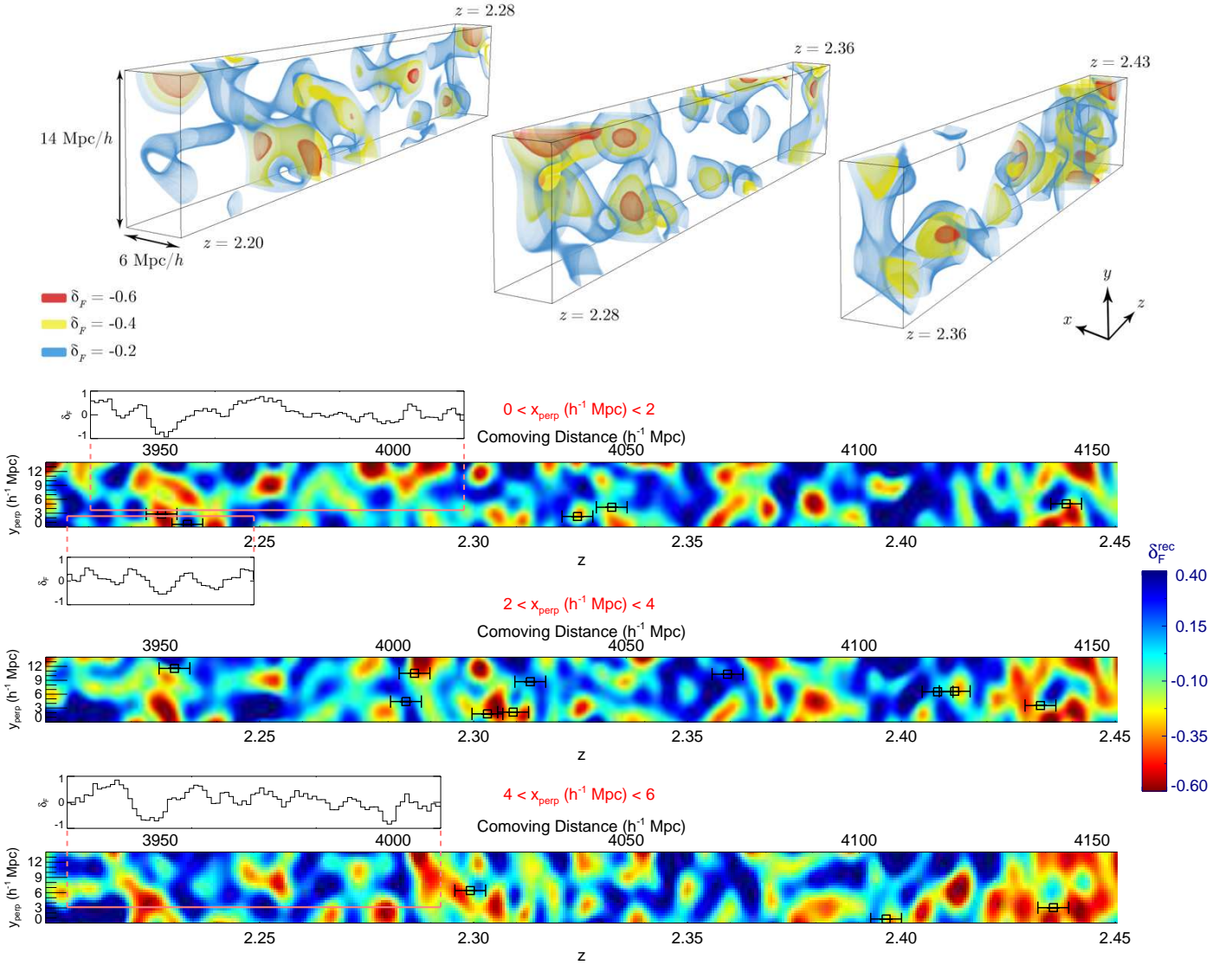


FIG. 3.— Tomographic reconstruction of 3D Ly α forest absorption from our data, shown in 3 redshift segments in 3D (top) and projected over 3 slices along the R.A. direction (bottom panels). The color scale represents reconstructed Ly α forest transmission such that negative values (red) correspond to overdensities. Square symbols denote positions of coeval galaxies within the map; error bars indicate the $\sigma_v \approx 300 \text{ km s}^{-1}$ uncertainty on their redshifts. Pink solid lines indicate where 3 of the skewers probe the volume, with inset panels indicating the corresponding 1D absorption spectra (top-hat smoothed by 3 pixels) that contributed to the tomographic reconstruction.

within our limited redshift range this effect is small.

The resulting map of the 3D Ly α forest absorption, δ_F^{rec} , is shown in Figure 3 as 3D visualizations and slices projected over the x_{perp} (R.A.) direction. A lot of structure is obvious even within this small volume, with overdensities (negative- δ_F^{rec} regions) spanning comoving distances of $\Delta y_{\text{perp}} \gtrsim 10 h^{-1} \text{ Mpc}$ both along the line-of-sight (e.g. from $z \approx 2.21$ to $z \approx 2.23$ at $y_{\text{perp}} \sim 8 h^{-1} \text{ Mpc}$) and across the transverse direction (at $z \approx 2.43$). The strong overdensities are typically sampled by multiple sightlines at different background redshifts. This is illustrated by inset panels in the map slices in Figure 3, where we show 3 examples of the 1D absorption field, δ_F , that went into the reconstruction — the overdensity at a comoving distance of $\approx 3950 h^{-1} \text{ Mpc}$ and $y_{\text{perp}} \leq 5 h^{-1} \text{ Mpc}$ can be seen as clear dips in all three of the spectra, which is unlikely to be caused by

pixel noise. Note that in moderate-resolution Ly α forest data, significant ‘absorbers’ are typically due to blends of clustered Ly α forest absorption and not individual absorbers (Lee et al. 2014b; Pieri et al. 2013). One also clearly sees significant voids (dark blue regions) on scales of $\sim 5 - 10 h^{-1} \text{ Mpc}$.

As validation, we performed reconstructions on mock data sets derived from simulations (e.g., L14). These mocks have identical sightline configurations, resolution, and S/N as the data, including random continuum errors with 7% RMS. The resulting reconstructions are illustrated in Figure 4, compared with the ‘true’ absorption field from the simulation. The good correspondence between large-scale features in the ‘true’ and reconstructed fields gives us confidence that the real map (Figure 3) is indeed probing LSS. However, the PDF of the simulated reconstructions differed from the real map (c.f. black

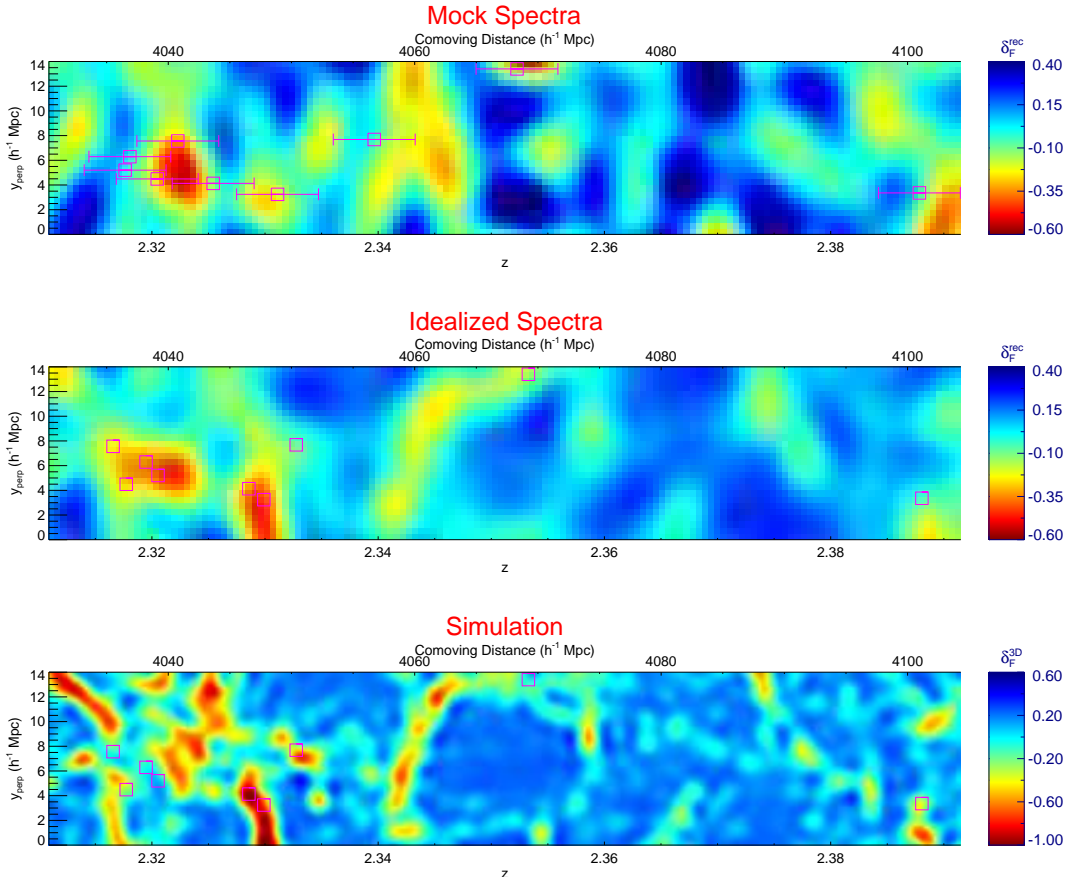


FIG. 4.— (Top) A slice from a tomographic reconstruction (projected over $\Delta x_{\text{perp}} = 2 h^{-1}$ Mpc) using a mock data set with similar spatial sampling and S/N to our data. (Middle) A reconstruction (with the same $[L_{\parallel}, L_{\perp}, \sigma_F]$) from the full grid of noiseless spectra with $0.8 h^{-1}$ Mpc transverse separations. For reference, the bottom panel shows the ‘true’ absorption field in the simulation. Magenta squares indicate locations of coeval $R \leq 25.5$ galaxies — in the top panel we also introduced random redshift errors.

histograms in Figures 5a and b). To investigate, we ran 24 mock reconstructions on independent simulation volumes, which showed considerable scatter in the resulting PDFs (shaded grey area in Figure 5b). This suggests that part of the discrepancy is due to cosmic-variance from our small volume. Moreover, while DM-only simulations correctly reproduce Ly α forest clustering, they do not yield the right PDF (White et al. 2010), which could also contribute to the disagreement.

L14 argue (e.g. their Figure 6) that the reconstructed δ_F^{rec} scales approximately linearly with the dark-matter overdensity, $\Delta_{\text{dm}} \equiv \rho_{\text{dm}}/\langle\rho_{\text{dm}}\rangle$, smoothed on similar scales ($\epsilon_{3\text{D}} \approx 3.5 h^{-1}$ Mpc in our case), albeit with some scatter due to reconstruction noise. The most negative δ_F^{rec} correspond to overdensities of $\Delta_{\text{dm}} \approx 2$ while the most positive δ_F^{rec} indicate underdensities of $\Delta_{\text{dm}} \approx 0.2$.

4. COMPARISON WITH COEVAL GALAXIES

Since galaxies are well-known tracers of LSS, we can exploit the spectroscopically-confirmed high-redshift galaxies within the COSMOS field (Lilly et al. 2007; Le Fevre et al. 2014) to make a comparison with our Ly α forest tomographic map. We searched an internal COSMOS compilation of all available spectroscopic redshifts, and found 18 galaxies coeval within the map volume (4 were uniquely confirmed by our observations). This small

number is clearly inadequate for mapping $z \gtrsim 2$ LSS on \sim Mpc scales, illustrating the challenge of using galaxy redshift surveys for this purpose, despite many hundred hours of large-telescope time. In order to make galaxy maps with comparable resolution to our tomographic reconstructions, the galaxy number density needs to be increased dramatically, requiring 30m-class telescopes to obtain redshifts from faint ($R \gtrsim 26$) galaxies.

For these coeval galaxies, we determined their 3D positions within our map (overplotted on Figure 3) and evaluated the corresponding δ_F^{rec} . The δ_F^{rec} sampled by these galaxies are shown in Figure 5a, compared with the δ_F^{rec} distribution from the full map; in Figure 5c, we show the galaxy distribution as a function of the percentile of map ranked by flux (where larger flux percentiles represent overdensities). The galaxies preferentially occupy low- δ_F^{rec} regions (i.e. overdensities) of the map.

However, at first glance it seems troublesome that several galaxies are located in high- δ_F^{rec} (underdense) regions. This could partly be due to errors in the galaxy spectroscopic redshifts: these are $\sigma_v \approx 300$ km s $^{-1}$ (Diener et al. 2013), i.e. $\sigma_{\chi} \approx 3.3 h^{-1}$ Mpc along the LOS at $z \approx 2.3$. This seems plausible for the galaxy at $[x_{\text{perp}}, y_{\text{perp}}, z] = [0.5 h^{-1}$ Mpc, $0.6 h^{-1}$ Mpc, 2.233] (top panel, Figure 3), which apparently occupies a void but is in fact within $\pm 1\sigma$ of two overdensities on either side. In-

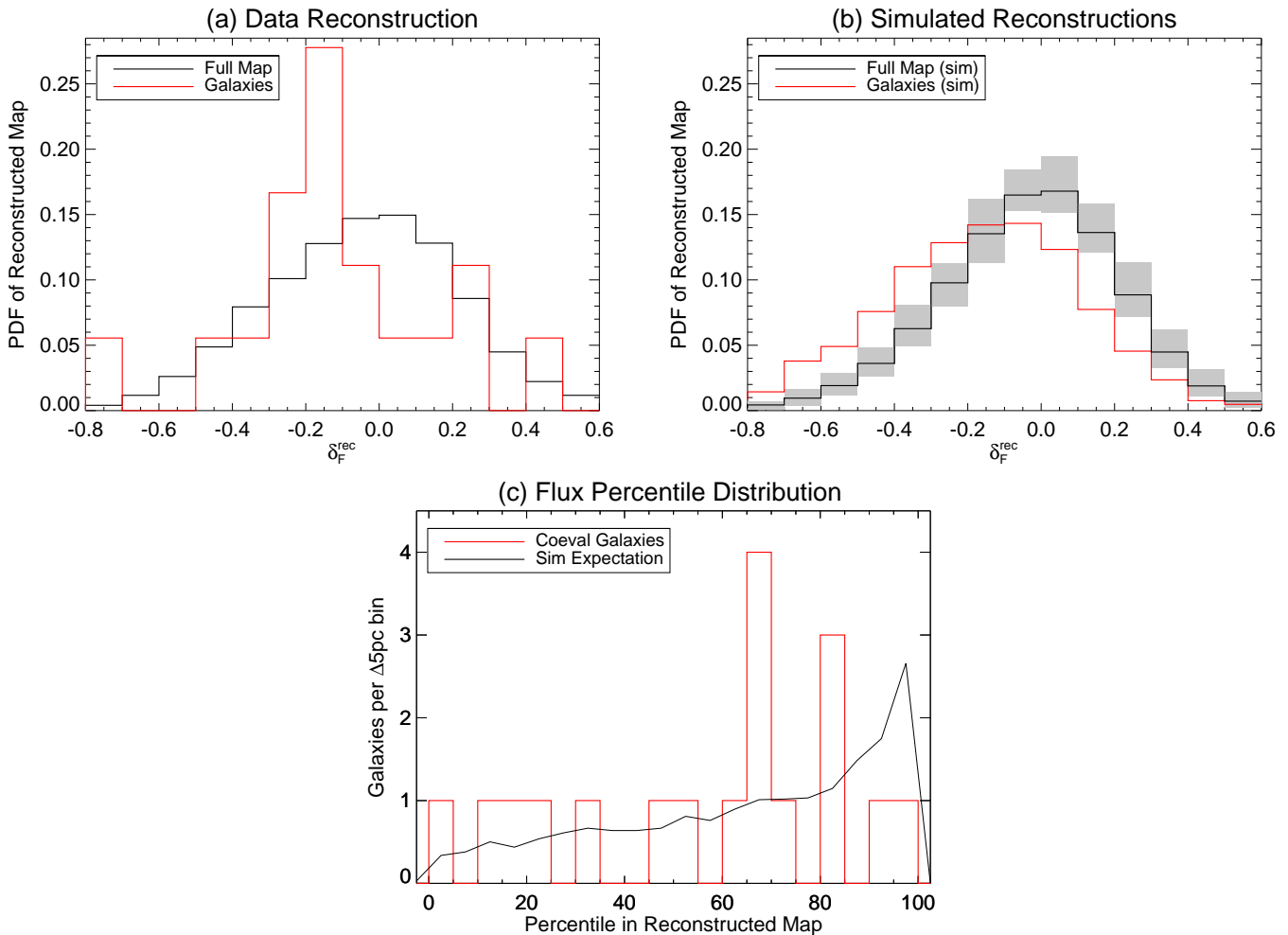


FIG. 5.— (a) PDF of our tomographic map (black) compared with that sampled by 18 coeval galaxies within our map volume (red, both PDFs normalized to unit area). (b) Similar to (a), but evaluated over 24 mock reconstructions simulating the real map. The red curve shows the δ_F^{rec} evaluated at 2506 simulated $R \leq 25.5$ galaxies within the mock reconstructions — the simulated galaxies clearly also preferentially live in low- δ_F^{rec} regions. Shaded regions indicate the range of map PDFs from the 24 mock reconstructions, indicating the significant sample variance from the small volume. (c) Distribution of coeval galaxies as a function of the map flux percentile, such that δ_F^{rec} decreases with the percentile, i.e. larger percentiles probe overdensities. The black curve indicates the predicted distribution from the simulated galaxies within our mock reconstructions.

deed, in Figure 3 most of the galaxies are within $\sim 1\sigma$ of significant overdensities. Another possible reason for this discrepancy could be different redshift-space distortions experienced by the galaxies and the forest: the latter has been constrained by Slosar et al. (2011) but yet to be measured for $z \gtrsim 2$ galaxies.

Tomographic reconstruction errors (c.f., Figure 4) could also decrease the correlation between the galaxies and 3D Ly α absorption, particularly in regions poorly-sampled by sightlines. We investigate this using our simulations, from which we extracted $R \leq 25.5$ galaxies through halo abundance-matching (see L14 for details), introduced the expected LOS redshift errors and then evaluated their positions within the mock tomographic reconstructions; this is illustrated by the mock galaxies in Figure 4. The distribution is shown in the red histogram in Figure 5b, which shows a clear preference towards negative- δ_F^{rec} (overdensities). This is also evident in Figure 5c, which shows the distribution as a function of flux percentiles (normalized to $N = 18$ as in the real data). A two-sample Kolmogorov-Smirnov test between

the percentile distribution of the real galaxies versus that from the simulations indicate 22% probability of being drawn from the same distribution, which is reasonable considering the small data set. The long tail of galaxies in the underdensities is primarily due to a combination of galaxy redshift errors and reconstruction noise. The former could be mitigated in the near-future by accurate systemic redshifts from near-IR spectroscopy, while to account for reconstruction noise we are developing methods to estimate the map covariance and hence characterize the uncertainties at any point within the maps.

5. CONCLUSION

We present the spectroscopic observations targeting, for the first time, high-redshift galaxies as background sources for Ly α forest analysis. This enabled us to create a tomographic map of the 3D absorption field with a spatial resolution of $\epsilon_{3D} \approx 3.5 h^{-1}$ Mpc covering a comoving volume of $\approx (27 h^{-1} \text{ Mpc})^3$ at $\langle z \rangle \approx 2.3$. Simulated tomographic reconstructions show that our sightline-sampling, resolution, and S/N should yield a

good recovery of the underlying absorption field. Supporting this conclusion, a sample of 18 coeval galaxies with known spectroscopic redshifts are found to preferentially occupy high-absorption regions (i.e. overdensities) in our map.

These results demonstrate the feasibility and promise of the full CLAMATO survey: ~ 1000 SFGs at $z_{\text{bg}} \sim 2 - 3$ covering $\sim 1 \text{ deg}^2$ in the COSMOS field, which will enable a $\langle z \rangle \sim 2.3$ Ly α forest tomographic map with $\epsilon_{3\text{D}} \sim 3 - 4 h^{-1}$ Mpc spatial resolution over a $(65 h^{-1} \text{ Mpc})^2 \times 250 h^{-1} \text{ Mpc} \sim (100 h^{-1} \text{ Mpc})^3$ comoving volume. This will allow us to directly characterize the topology and morphology of $z > 2$ LSS for the first time — already we see tantalizing hints of structures extending across $\gtrsim 10 h^{-1}$ Mpc in the high-redshift cosmic web. A large-volume LSS map will also enable a search for progenitors of massive $z \sim 0$ galaxy clusters — these protoclusters should manifest themselves at $z \gtrsim 2$ as overdensities of a few over $\sim 10 h^{-1}$ Mpc (Chiang et al. 2013) scales. In a forthcoming paper, we will discuss methods to find protoclusters using Ly α forest tomography.

The proposed survey will create rich synergy with other

COSMOS datasets. We would be able to study various high-redshift galaxy properties, e.g., morphology, color, star-formation rate, as a function of their environment within the cosmic web. Such studies will require the full $\sim (100 h^{-1} \text{ Mpc})^3$ CLAMATO volume in order to sample enough objects to beat down the galaxies' redshift uncertainties and reconstruction errors, but promises unique insights into galaxy formation and evolution during the $z \sim 2 - 3$ epoch. Finally, CLAMATO will probe small-scale clustering of LSS, and will be highly-complementary with wide-field surveys such as HETDEX (Hill et al. 2004) and DESI (Levi et al. 2013) to probe cosmological clustering over a broad range of spatial-scales at $z \gtrsim 2$.

KGL and ACE are grateful to the National Geographic Society for travel support through the Waitt Grants program. This research used resources of the NERSC Center, which is supported by the Office of Science of the U.S. D.O.E. under Contract #DE-AC02-05CH11231. We would like to thank those of Hawai'ian ancestry, on whose sacred mountain we were privileged to be guests.

REFERENCES

- Becker, G. D., Hewett, P. C., Worseck, G., & Prochaska, J. X. 2013, MNRAS, 430, 2067
- Berry, M., Gawiser, E., Guaita, L., et al. 2012, ApJ, 749, 4
- Bi, H., Ge, J., & Fang, L.-Z. 1995, ApJ, 452, 90
- Brammer, G. B., van Dokkum, P. G., Franx, M., et al. 2012, ApJS, 200, 13
- Busca, N. G., Delubac, T., Rich, J., et al. 2013, A&A, 552, A96
- Capak, P., Aussel, H., Ajiki, M., et al. 2007, ApJS, 172, 99
- Caucchi, S., Colombi, S., Pichon, C., et al. 2008, MNRAS, 386, 211
- Cen, R., Miralda-Escudé, J., Ostriker, J. P., & Rauch, M. 1994, ApJ, 437, L9
- Chiang, Y.-K., Overzier, R., & Gebhardt, K. 2013, ApJ, 779, 127
- Cisewski, J., Croft, R. A. C., Freeman, P. E., et al. 2014, MNRAS, 440, 2599
- Croft, R. A. C., Weinberg, D. H., Bolte, M., et al. 2002, ApJ, 581, 20
- Croft, R. A. C., Weinberg, D. H., Katz, N., & Hernquist, L. 1998, ApJ, 495, 44
- Dawson, K. S., Schlegel, D. J., Ahn, C. P., et al. 2013, AJ, 145, 10
- Delubac, T., Bautista, J. E., Busca, N. G., et al. 2014, arXiv:1404.1801
- Diener, C., Lilly, S. J., Knobel, C., et al. 2013, ApJ, 765, 109
- Hill, G. J., Gebhardt, K., Komatsu, E., & MacQueen, P. J. 2004, in American Institute of Physics Conference Series, Vol. 743, The New Cosmology: Conference on Strings and Cosmology, ed. R. E. Allen, D. V. Nanopoulos, & C. N. Pope, 224–233
- Hui, L., Gnedin, N. Y., & Zhang, Y. 1997, ApJ, 486, 599
- Ilbert, O., Capak, P., Salvato, M., et al. 2009, ApJ, 690, 1236
- Koekemoer, A. M., Aussel, H., Calzetti, D., et al. 2007, ApJS, 172, 196
- Le Fevre, O., Tasca, L. A. M., Cassata, P., et al. 2014, arXiv:1403.3938
- Lee, K.-G., Hennawi, J. F., White, M., Croft, R. A. C., & Ozbek, M. 2014a, ApJ, 788, 49
- Lee, K.-G., Suzuki, N., & Spergel, D. N. 2012, AJ, 143, 51
- Lee, K.-G., Bailey, S., Bartsch, L. E., et al. 2013, AJ, 145, 69
- Lee, K.-G., Hennawi, J. P., Spergel, D. N., et al. 2014b, arXiv:1405.1072
- Leitherer, C., Ortiz Otálvaro, P. A., Bresolin, F., et al. 2010, ApJS, 189, 309
- Leitherer, C., Schaerer, D., Goldader, J. D., et al. 1999, ApJS, 123, 3
- Levi, M., Bebek, C., Beers, T., et al. 2013, arXiv:1308.0847
- Lilly, S. J., Le Fèvre, O., Renzini, A., et al. 2007, ApJS, 172, 70
- McDonald, P., Seljak, U., Burles, S., et al. 2006, ApJS, 163, 80
- Oke, J. B., Cohen, J. G., Carr, M., et al. 1995, PASP, 107, 375
- Palanque-Delabrouille, N., Yèche, C., Borde, A., et al. 2013, A&A, 559, A85
- Pichon, C., Vergely, J. L., Rollinde, E., Colombi, S., & Petitjean, P. 2001, MNRAS, 326, 597
- Pieri, M. M., Mortonson, M. J., Frank, S., et al. 2013, arXiv:1309.6768
- Press, W. H., Teukolsky, S. A., Vetterling, W. T., & Flannery, B. P. 1992, Numerical recipes in FORTRAN. The art of scientific computing (Cambridge University Press)
- Reddy, N. A., Steidel, C. C., Pettini, M., et al. 2008, ApJS, 175, 48
- Salvato, M., Ilbert, O., Hasinger, G., et al. 2011, ApJ, 742, 61
- Savaglio, S., Panagia, N., & Padovani, P. 2002, ApJ, 567, 702
- Scoville, N., Aussel, H., Brusa, M., et al. 2007, ApJS, 172, 1
- Shapley, A. E., Steidel, C. C., Pettini, M., & Adelberger, K. L. 2003, ApJ, 588, 65
- Slosar, A., Font-Ribera, A., Pieri, M. M., et al. 2011, JCAP, 9, 1
- Steidel, C. C., Shapley, A. E., Pettini, M., et al. 2004, ApJ, 604, 534
- White, M., Pope, A., Carlson, J., et al. 2010, ApJ, 713, 383
- Wiener, N. 1942, 'The interpolation, extrapolation and smoothing of stationary time series' (MIT)
- Zaroubi, S., Hoffman, Y., Fisher, K. B., & Lahav, O. 1995, ApJ, 449, 446